

Quantitative comparison of filtering methods in lattice QCD

Falk Bruckmann¹, Christof Gattringer², Ernst-Michael Ilgenfritz³, Michael Müller-Preussker³, Andreas Schäfer¹, Stefan Solbrig¹

¹ Institut für Theoretische Physik, Universität Regensburg, D-93040 Regensburg, Germany

² Institut für Physik, FB Theoretische Physik, Universität Graz, A-8010 Graz, Austria

³ Humboldt-Universität zu Berlin, Institut für Physik, Newtonstr. 15, D-12489 Berlin, Germany

Received: date / Revised version: date

Abstract We systematically compare filtering methods used to extract topological excitations (like instantons, calorons, monopoles and vortices) from lattice gauge configurations, namely APE-smearing and spectral decompositions based on lattice Dirac and Laplace operators. Each of these techniques introduces ambiguities, which can invalidate the interpretation of the results. We show, however, that all these methods, when handled with care, reveal very similar topological structures. Hence, these common structures are free of ambiguities and faithfully represent infrared degrees of freedom in the QCD vacuum. As an application we discuss an interesting power-law for the clusters of filtered topological charge.

PACS. 1 2.38.-t Quantum chromodynamics – 1 2.38.Gc Lattice QCD calculations – 1 1.15.Ha Lattice gauge theory

1 Introduction

Ever since the advent of quantum chromodynamics (QCD) its infrared properties have been of primary interest. One of the most important phenomena in this regime is the confinement of quarks. As a typical nonperturbative effect it still calls for a derivation from first principles, even for pure gauge theory (where it reveals itself as, e.g., an area law for the Wilson loop).

Remarkably, most of the most popular nonperturbative approaches to the QCD vacuum have been around for quite some time now. Topological excitations like instantons, calorons, magnetic monopoles and vortices have been used for semiclassical and condensed matter-inspired models since the 70's [1]. In spite of the successes of these models, the question of their relevance for confinement is the subject of debate.

Lattice gauge theory (LGT) is of roughly the same age and till today the only nonperturbative and systematically improvable regulator of QCD. Thus it has the potential to lend support to and to decide between the various models.

However, the QCD vacuum on the lattice as seen by naive gluonic observables has been found to be dominated by ultraviolet (size $O(a)$) fluctuations and therefore it is difficult to make contact to continuum models. To deal with this problem, various smoothing procedures, filtering out the UV 'noise', have been developed and applied to lattice configurations. It has been objected that physical properties could be lost and unphysical artefacts may be generated by these filtering methods. Both effects would strongly spoil the conclusions, for instance w.r.t. the ex-

tracted density of the building blocks, drawn from any such study.

In this work we systematically investigate the most common and a priori quite different procedures to filter lattice configurations, namely smearing and the modern methods based on the eigenmodes of lattice Dirac and Laplace operators.

We find a surprisingly strong agreement of the topological content of configurations in thermal equilibrium seen through the different methods. We show how the parameters of the latter can be adapted systematically. This knowledge forms a very important prerequisite to uniquely identify the structure of the QCD vacuum.

2 Filtering methods

Smearing and the related method of cooling have often been used to improve the signal in observables or to obtain smoother link variables as input for lattice operators. For definiteness here we will use a 4D version of APE-smearing, that has been argued to be equivalent to RG cycling [2]. It is an iterative procedure, where links are replaced by a weighted average of the links and the staples $U_\mu^\nu(x) = U_\nu(x)U_\mu(x + \hat{\nu})U_\nu^\dagger(x + \hat{\mu})$ surrounding it:

$$U_\mu(x) \rightarrow \mathcal{P}[\alpha U_\mu(x) + \gamma \sum_{\nu \neq \mu} U_\mu^\nu(x)]. \quad (1)$$

Here \mathcal{P} denotes the projection onto the gauge group (for $SU(2)$ just a rescaling of the matrix by a scalar). We

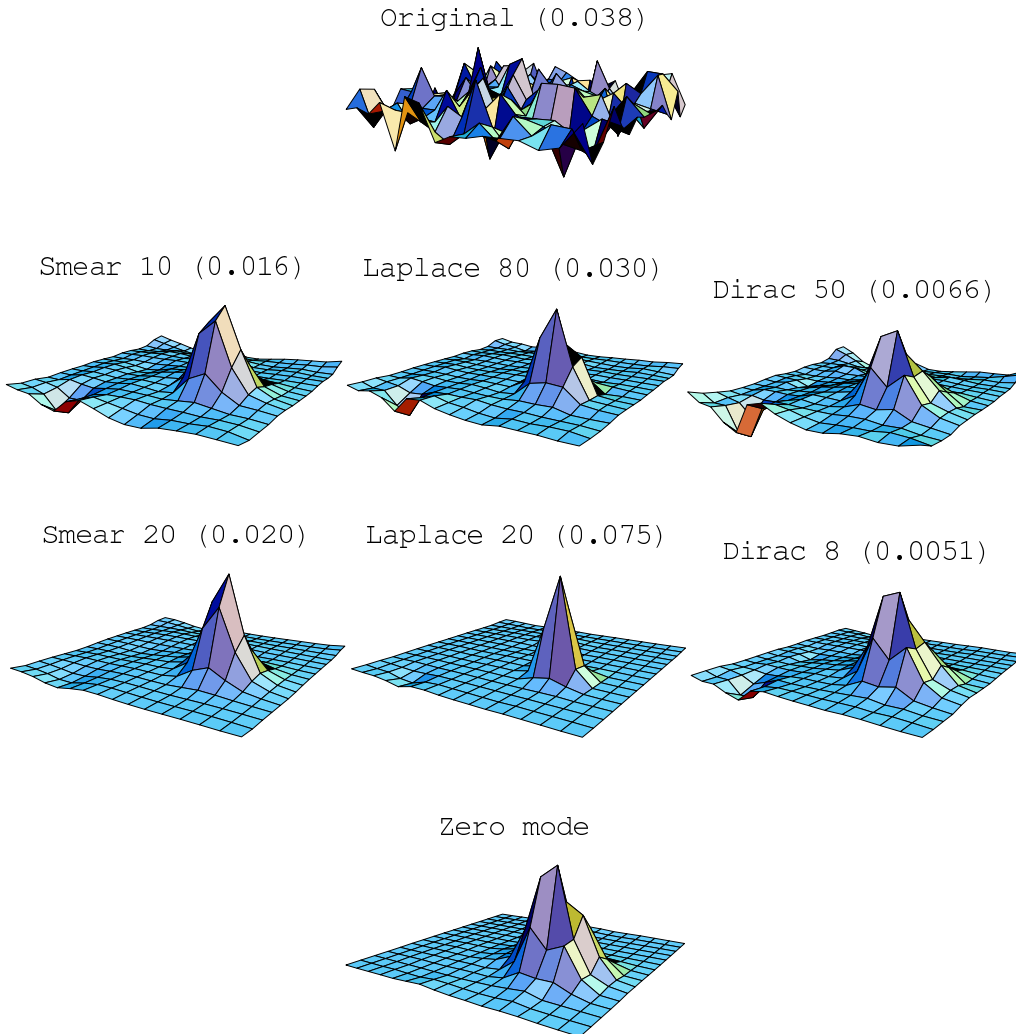


Figure 1. Effect of different filtering methods on the topological density for a particular $Q = 1$ configuration in a fixed lattice plane. On top we show the original topological density. In the second and third row one sees the effects of smearing (first column) and Laplace filtering (second column) as well as the topological density in terms of Dirac eigenmodes (last column). At the bottom the profile of the chiral zero mode is shown for the combined filtering methods. (The numbers in brackets give the heights of the corresponding maxima.)

choose $\alpha = 0.55$ and $\gamma = 0.075$, following [2]. Cooling is obtained by ignoring the old link ($\alpha = 0$) and is known to drive the configurations towards classical solutions. We update one link at a time, but as the weight of the central link is quite high, our technique qualifies as smearing rather than cooling.

A more recent idea for filtering is to use eigenmodes of lattice Dirac operators. Generally speaking, their function as filters is based on the argument that low-lying eigenmodes tend to be smooth, see Fig. 1 for an example. The positions revealed by the lowest-lying modes are expected to be correlated with the location of the relevant gluonic IR excitations, in particular of topological objects [3]. Whether peaks show up at the same locations when gluonic filtering methods are applied, is an important consistency check for the latter.

The *Dirac filtering* method relies on the representation of gluonic observables through eigenmode expansions of lattice Dirac operators (see also [4]). In the following we will investigate the topological charge density [5] in terms of eigenmodes of a Ginsparg-Wilson type Dirac operator D :

$$q(x) = \text{tr} \gamma_5 \left(\frac{1}{2} D_{x,x} - 1 \right) = \sum_{n=1}^N \left(\frac{\lambda_n}{2} - 1 \right) \psi_n^\dagger(x) \gamma_5 \psi_n(x) \quad (2)$$

which is exact for $N = \text{Vol} \cdot 4N_c$ and can be truncated for filtering purposes at low N [6]. The total topological charge $Q = \sum_x q(x)$ is an integer given by the contributions of chiral zero modes, whereas the non-zero modes modify the local distribution $q(x)$ only.

The third filtering method we use is the *Laplace filter* that represents link variables through a spectral sum [7]

$$U_\mu(x) = \mathcal{P} \sum_{n=1}^N (16 - 2\lambda_n) \phi_n(x) \otimes \phi_n^\dagger(x + \hat{\mu}). \quad (3)$$

Here, ϕ_n are the eigenmodes of the gauge covariant Laplace operator $-D^2[U]$ with eigenvalues λ_n , of which again only the lowest N are taken into account. In the limit $N = \text{Vol} \cdot N_c$ the original links would be reproduced. Numerically this filter is cheaper than Dirac operators.

The strength of the filters can be controlled. More iterations of smearing or fewer eigenmodes result in a stronger filtering. We also remark that smearing is a strictly local procedure, while working with eigenmodes introduces an intrinsic nonlocality, the consequences of which are not fully understood yet.

3 Results

We have generated 295 independent quenched $SU(2)$ configurations on a 16^4 lattice with tree-level Lüscher-Weisz action at $\beta = 1.95$ (the lattice spacing is $a = 0.075(1) fm$). We use chirally improved fermions [8], an approximate solution of the Ginsparg-Wilson relation, which reveal chiral properties well enough without the big computational demands of, e.g., overlap fermions.

The main physical observable for our comparative study is the topological charge density. For smearing and the Laplace method, which both provide filtered links, we use the gluonic definition $q(x) = \sum_{\mu,\nu} \text{tr} F_{\mu\nu} \tilde{F}_{\mu\nu} / 16\pi^2$ with an improved field strength $F_{\mu\nu}$ constructed from 1×1 , 2×2 and 3×3 Wilson loops [9]. The Dirac eigenmodes yield $q(x)$ directly via Eq. (2).

In Fig. 1 we show the result of the three methods realizing two levels of filtering (mild and strong, see later) on a thermalized $Q = 1$ configuration in a fixed lattice plane. It shows an excellent agreement of the ‘hot spots’, i.e., lattice locations with large local topological charge, visible through the various methods. For mild filtering also less pronounced structures appear, which agree between the methods (and are washed out by strong filtering).

Moreover, the most pronounced structure corresponds to a maximum in the profile of the chiral zero mode. From this consistency we can conclude qualitatively that differences between the methods are small.

The configuration used in Fig. 1 has unit topological charge, following from the existence of a single chiral zero mode. The following table shows in as far smearing and Laplace filtering recover this fact:

The main conclusion here is that the three methods point to the same total charge $Q = 1$. Furthermore, Q evaluated after smearing approaches unity rather quickly and then becomes stable. It also keeps the chiral zero mode (marked with asterisks * in the table). The Laplace-filtered configurations, on the other hand, are not arbitrarily smooth, such that the gluonic topological charge measured on them is 1 within some margin; on the configurations filtered with

sweeps	smearing	Laplace filtering	
	Q	Q	modes
1	0.948*	1.161*	160
2	1.256*	0.947*	80
5	1.118*	0.896*	40
10	1.004*	0.778*	20
20	1.000*	0.760*	10
80	1.000*	-0.138	4

10 or more modes we find again one chiral zero mode confirming $Q = 1$.

The example discussed so far is typical for the whole ensemble (including all Q -values) and helps one to visualize the impressive similarity of smearing, Laplace filtering and Dirac eigenmodes, which in the following will be quantified.

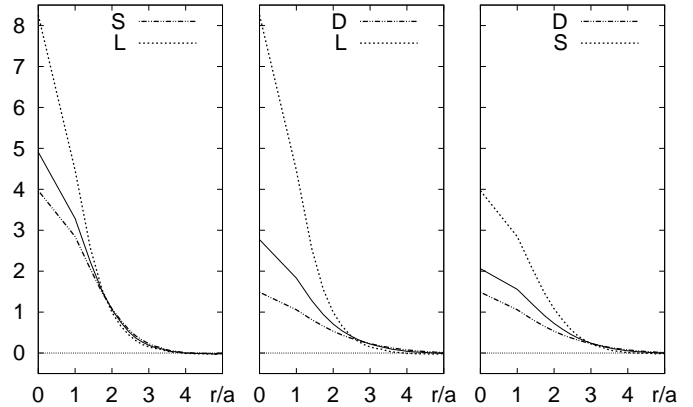


Figure 2. Auto-correlators $\chi_{AA}(r)$ (broken lines) and cross-correlators $\chi_{AB}(r)$ (full line) of smearing (S), Laplace (L) and Dirac (D) filtering for the configuration of Fig. 1 at mild filtering. The unit on the vertical axis is 10^{-7} .

In particular we try to set the parameters of the filtering methods such that the results match as well as possible. For that purpose we consider correlators of the topological charge density (with its average $\bar{q} = Q/\text{Vol}$ subtracted):

$$\chi_{AB}(r) = \frac{\sum_{x,y} (q_A(x) - \bar{q}_A)(q_B(y) - \bar{q}_B) \delta(|x-y| - r)}{\sum_{x,y} \delta(|x-y| - r)} \quad (4)$$

depending on the four-dimensional distance r . A and B stand for the filtering methods under consideration (including their parameters).

As Fig. 2 shows, the auto-correlators $\chi_{AA}(r)$ have a positive profile over a few lattice spacings followed by a slightly negative tail, and the cross-correlators $\chi_{AB}(r)$ fall in between them. The ratio of the latter to the geometric mean, $\Xi_{AB} = \chi_{AB}^2(0) / (\chi_{AA}(0)\chi_{BB}(0))$, being close to 1 signals local agreement between the topological charge landscapes of methods A and B .

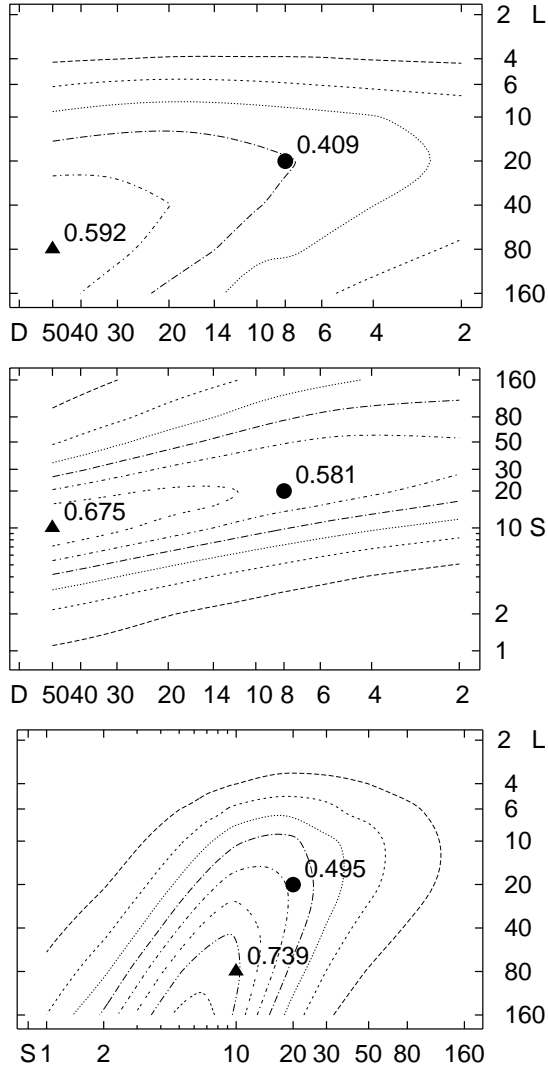


Figure 3. Level curves $\Xi_{AB} = 0.1, 0.2, \dots$ (inwards) for A and B being smearing sweeps (S), Laplacian (L) and Dirac (D) eigenmodes, averaged over 10 configurations. The parameter sets we use at mild and strong filtering are indicated by a full triangle and a circle, respectively.

Fig. 3 shows Ξ_{AB} for pairwise comparisons of smearing, Laplacian and Dirac filtering¹. In all pairs of methods Ξ_{AB} reveals a ‘ridge’ on which the parameters match best. From mild filtering (lower left corner²) to stronger filtering (upper right corner) the methods deviate from each other and the height of the ridge decreases. Two optimal parameter sets chosen from that figure (and indicated in it) are used in due course:

¹ Investigations that need 50 Dirac modes are done on an ensemble of 10 configurations for computational reasons.

² From the definition it follows that in the limit of no smearing sweeps vs. $\text{Vol} \cdot N_C$ Laplacian modes one has $\Xi_{AB} = 1$.

	smearing	Laplace	Dirac
mild filtering	10 sweeps	80 modes	50 modes
strong filtering	20 sweeps	20 modes	8 modes

These matchings have also been confirmed by comparing smeared and Laplace-filtered links minimizing

$$\sum_{x,\mu} \text{tr} (U_\mu^A(x) - U_\mu^B(x))^\dagger (U_\mu^A(x) - U_\mu^B(x)) \quad .$$

For these two optimized parameter sets we summarize in the following table some additional measurements, which characterize the deviation of the smeared and Laplace-filtered ensemble from the original Monte Carlo one (295 configurations). The observables are the percentage of configurations for which the topological charge Q coincides with the number of zero modes (called Q_D) and the decrease of the action S :

	$ Q - Q_D \leq 0.5$	S/S_{orig}
10 sweeps	89%	0.026
80 modes	76%	0.036
20 sweeps	85%	0.009
20 modes	69%	0.017

In reducing the noise, the action has been reduced by approximately two orders of magnitude, while the string tension is unchanged within errors.

With the parameter sets at hand we further quantify the local agreement of the methods by looking at clusters of filtered topological charge. For each method A , cuts in the topological charge density are adjusted such that the sets X_A of points above the cut have the same volume fraction $f = \text{vol}(X_A)/\text{Vol}$. Then we compare the volume in the overlap (with same sign of topological charge) vs. the union of pairs X_A and X_B to obtain the relative point overlap (RPO) s_{AB} :

$$s_{AB} = \sum_{\substack{x \in X_A \cap X_B \\ q_A(x)q_B(x) > 0}} 1 / \sum_{x \in X_A \cup X_B} 1. \quad (5)$$

In Fig. 4 upper panel the RPOs are plotted against the volume fraction f . The main result to emphasize here is that the pairwise point overlaps are large, typically 50% to 60%, and constant over a wide range of f , which implies that also the shapes of the topological lumps agree.

Based on our analysis we are able to discard ambiguities of the individual methods. When we analyze only points that are common to all three methods, the number of clusters is reduced accordingly, see Fig. 4 lower panel.

Intermediate values of f are suited for a cluster analysis as they contain enough statistics and avoid cluster mergings. Interestingly, in that regime we find for the common structures a pronounced *power-law for the number of clusters as a function of f* . In order to better interpret this behavior, we will discuss in the next section gross features of a class of models including the dilute instanton gas that predict such a power-law.

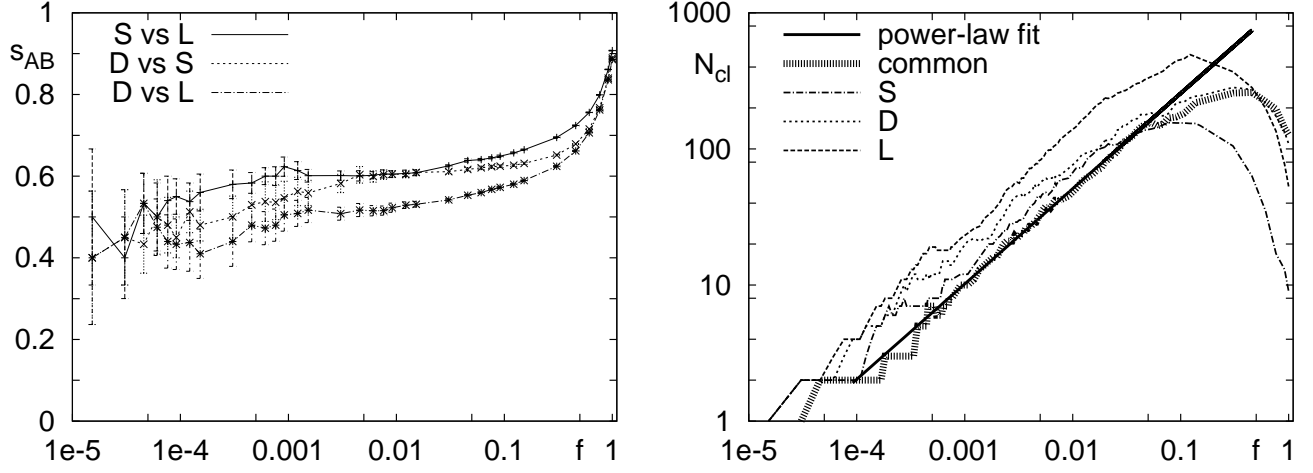


Figure 4. RPOs averaged over 10 configurations (left) and the number of clusters for the configuration of Fig. 1 (right, logarithmically, including a power-law fit), both as a function of the volume fraction f at mild filtering.

4 A model for the power-law

We are now considering models of topological lumps in the continuum. The latter are assumed to be dilute and described by an arbitrary shape function F with size parameter ρ :

$$q(r) = F(r/\rho) \rho^{-\delta}. \quad (6)$$

When applying cuts to the topological charge density, it is useful to characterize the lumps by their maximum

$$q_0 \equiv q(0) = F(0)\rho^{-\delta}. \quad (7)$$

Let us assume a power-law distribution of size parameters $d(\rho) \sim \rho^\beta$, which can be translated into a power-law distribution of maxima

$$d(q_0) \sim q_0^{-\alpha}, \quad \alpha = (\beta + \delta + 1)/\delta. \quad (8)$$

Then the number of clusters visible above a cut q is simply

$$N_{\text{clust}}(q) = \int_q^\infty dq_0 d(q_0) \sim q^{1-\alpha}. \quad (9)$$

The next step is to compute the total volume of these clusters. We assume that r is a d -dimensional radius. Then for a single cluster (with maximum q_0) we obtain the following volume above q :

$$\begin{aligned} V(q_0, q) &= \int d^{d-1}\Omega \int_0^\infty dr r^{d-1} \theta(q(r) - q) \\ &\sim \rho^d F^{-1}(q\rho^\delta) \sim q_0^{-d/\delta} F^{-1}(F(0)q/q_0). \end{aligned} \quad (10)$$

Hence the total volume or equivalently the total number of lattice points with topological charge density above the cut q can be calculated to

$$N_{\text{points}}(q) = \int_q^\infty dq_0 d(q_0) V(q, q_0) \sim q^{1-\alpha-d/\delta}. \quad (11)$$

Together with (8,9) this predicts the following exponent

$$\xi \equiv \frac{d \log N_{\text{clust}}(q)}{d \log N_{\text{points}}(q)} = \frac{1}{1 + d/(\beta + 1)}, \quad (12)$$

independently of the actual profile F .

For the naive dilute instanton ensemble the various parameters are $d = \delta = 4$ and $\beta = 11N_c/3 - 5 = 7/3$, yielding $\xi = 5/11$ (the precise way of cutting off the instanton size distribution at large ρ will not matter since we are concentrating on hot spots of large topological charge density, i.e. small size).

Tests with toy models of lumps show that the detection of the power-law and its coefficient ξ hardly depends on finite volume or finite lattice spacing, as long as the lumps are dilute. However, a high density of topological objects modifies ξ . In the extreme case of the topological charge density being pure noise one obtains $\xi = 1$, as every cluster comes with just one point.

The measured exponent for the topological charge density indeed is close to 1 for very mild or no filtering. As Fig. 5 shows, ξ is lowered when removing noise by filtering and tends to a plateau for moderate filter parameters. At strong filtering the cluster statistics becomes unreliable since the topological landscape is dominated by very few clusters.

In order to avoid ambiguities of the different methods, we have based our analysis on clusters common to smearing and Laplacian modes (neglecting the numerically expensive Dirac eigenmodes). In the upper panel of Fig. 5 we depict ξ along the ridge of optimally matching parameters, whereas in the lower panel of that figure we include other (non-optimal) pairs of parameters.

While the statistical errors of the fits are small, the systematic errors from choosing the f -interval for the power-law are hard to quantify. Estimating the latter we obtain the following value of the power-law exponent

$$\xi = 0.59(5) \quad (13)$$

for the filtered lumps of topological charge density.

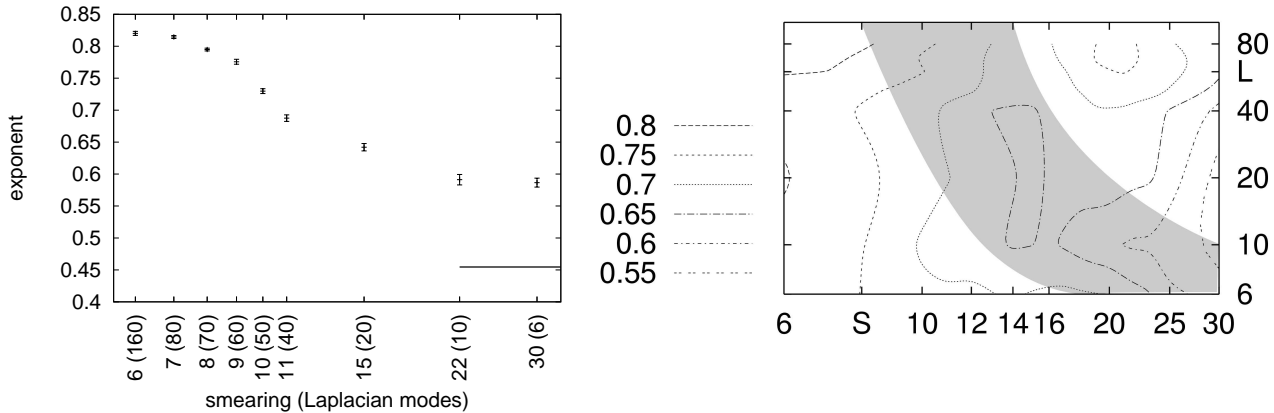


Figure 5. The exponent ξ of common topological clusters as a function of smearing sweeps and Laplacian modes. The best matching parameters (cf. Fig. 3 right) are used in the left plot and marked by a grey band in the right plot.

This result certainly excludes the simplest dilute gas of instantons (for which $\xi = 0.45$ see above, included in Fig. 5 top) as primary topological structures. This is not surprising, as instanton ensembles are expected to be non-dilute. For other scenarios the expected behavior depends crucially on the specific model assumptions. Therefore, we leave it to the proponents of any such model to check whether it is in agreement with our findings.

5 Conclusions

We have presented a systematic comparison of filtering methods on the lattice, namely the gluonic smearing update and truncated expansions based on Laplacian and Dirac eigenmodes. Our finding, that these filtering methods agree surprisingly well, allows us to identify structures of interest nearly free of ambiguities.

As a general rule, smearing – which is the cheapest method – represents these objects reasonably well. In order to control its effects, however, we consider it essential to compare several filtering methods. To this end we have shown how to match the parameters of the methods optimally.

As a first application we have measured a power-law for the number of filtered clusters and presented a class of models in which the corresponding exponent is a function of the size distribution coefficient and the dimensionality. We have found that the measured exponent cannot be interpreted in terms of a dilute instanton gas.

This work has been supported by DFG (Forschergruppe ‘Gitter-Hadronen-Phänomenologie’) and BMBF.

References

1. G. 't Hooft, Saalburg lecture notes (2000) hep-th/0010225.

2. T. DeGrand, A. Hasenfratz, and T. G. Kovacs, Nucl. Phys. **B520**, (1998) 301.
3. C. Gattringer, E.-M. Ilgenfritz, and S. Solbrig, (2006); hep-lat/0601015.
4. C. Gattringer, Phys. Rev. Lett. **88** (2002) 221601.
5. F. Niedermayer, Nucl. Phys. Proc. Suppl. **73** (1999) 105.
6. I. Horvath et al., Phys. Rev. **D67** (2003) 011501; Phys. Rev. **D68** (2003) 114505; E.-M. Ilgenfritz et al., Nucl. Phys. Proc. Suppl. **153** (2006) 328.
7. F. Bruckmann and E.-M. Ilgenfritz, Phys. Rev. **D72** (2005) 114502.
8. C. Gattringer, Phys. Rev. **D63** (2001) 114501; C. Gattringer, I. Hip, and C. Lang, Nucl. Phys. **B597** (2001) 451.
9. S. O. Bilson-Thompson, D. B. Leinweber, and A. G. Williams, Ann. Phys. **304** (2003) 1.

